JOURNAL OF GEOPHYSICAL RESEARCH, VOL. 108, NO. A12, 1435, doi:10.1029/2003JA009958, 2003

Spatial and temporal variability of the gamma radiation from Earth's atmosphere during a solar cycle

Michael J. Harris
Universities Space Research Association, Washington, D.C., USA

Gerald H. Share
Naval Research Laboratory, Washington, D.C., USA

Mark D. Leising
Department of Physics and Astronomy, Clemson University, Clemson, South Carolina, USA

Received 25 March 2003; revised 11 August 2003; accepted 14 August 2003; published 12 December 2003.

[1] The Solar Maximum Mission satellite's Gamma Ray Spectrometer spent much of its 1980–1989 mission pointed at Earth, accumulating spectra of atmospheric albedo γ-rays. Its 28° orbit ensured that a range of geomagnetic latitudes was sampled. We measured the variation with time and cutoff rigidity of some key γ-ray lines which are diagnostic of the intensity of the Galactic cosmic radiation penetrating the geomagnetic cutoff and of the secondary neutrons produced in the atmosphere. We found that the intensities of nuclear lines at 1.6 MeV, 2.3 MeV and 4.4 MeV varied inversely with solar activity in cycles 21–22 as expected from the theory of solar modulation of cosmic rays. They were found to be strongly anticorrelated with cutoff rigidity, as expected from the theory of the cutoff, falling by a factor ~3.6 between the lowest (<7 GV) and highest (>13 GV) rigidities sampled. The solar cycle modulation was particularly marked at the lowest rigidities, reaching an amplitude of 16%. The ratios of the intensities of the lines produced by nuclear de-excitation (1.6 MeV, 2.3 MeV) and those from nuclear spallation (4.4 MeV) did not vary with either solar activity or cutoff rigidity, indicating that the shape of the secondary neutron spectrum in the atmosphere above 5 MeV was approximately constant over the times and regions sampled. If it is approximated by a power law in energy, we derive constraints on the absolute value of the power law index $\sim -1.15 - -1.45$ and better constraints on its variability, $\leq 5\%$ over a solar cycle, and $\leq 6\%$ over SMM's range of sampled cutoff rigidities. We also measured the intensity of the electron-positron annihilation line at 0.511 MeV. This line also varies with the solar cycle, but its variation with cutoff rigidity is weaker than that of the nuclear lines, falling by a factor 2 (rather than 3.6) over SMM's range of sampled cutoff rigidities. This can be understood in terms of the energy dependences of the cross sections for positron production and for the hadronic interactions which produce secondary neutrons. *INDEX TERMS:* 7554 Solar Physics, Astrophysics, and Astronomy: X rays, gamma rays, and neutrinos; 2104 Interplanetary Physics: Cosmic rays; 7536 Solar Physics, Astrophysics, and Astronomy: Solar activity cycle (2162); 7837 Space Plasma Physics: Neutral particles; *KEYWORDS:* Earth atmosphere neutrons, X rays, gamma rays, solar activity cycle, energetic particles

Citation: Harris, M. J., G. H. Share, and M. D. Leising, Spatial and temporal variability of the gamma radiation from Earth's atmosphere during a solar cycle, *J. Geophys. Res.*, *108*(A12), 1435, doi:10.1029/2003JA009958, 2003.

1. Introduction

[2] A significant contribution to the radiation environment in low Earth orbit (LEO) consists of γ-radiation emitted by the atmosphere. These so-called albedo photons are the ultimate products of impacts by high energy cosmic ray particles on the nuclei of atoms in the upper atmosphere. Earth's magnetic field shields these layers to some extent from charged particles, especially the relatively soft-spectrum flux of protons from the Sun. The more energetic particles in the Galactic cosmic radiation (GCR) are therefore responsible for the long-term quiescent atmospheric γ-radiation, away from times of discrete solar flaring and coronal mass ejection events.

[3] The intensity of the quiescent γ-ray flux is expected to vary both spatially and temporally as a result of modu-

0148-0227/03/2003JA009958$09.00

Report Documentation Page

Form Approved
OMB No. 0704-0188

1. REPORT DATE	2. REPORT TYPE	3. DATES COVERED
12 DEC 2003		**00-00-2003 to 00-00-2003**

4. TITLE AND SUBTITLE	5a. CONTRACT NUMBER
Spatial and temporal variability of the gamma radiation from Earth?s atmosphere during a solar cycle	5b. GRANT NUMBER
	5c. PROGRAM ELEMENT NUMBER
6. AUTHOR(S)	5d. PROJECT NUMBER
	5e. TASK NUMBER
	5f. WORK UNIT NUMBER
7. PERFORMING ORGANIZATION NAME(S) AND ADDRESS(ES) **Naval Research Laboratory,E. O. Hulburt Center for Space Research,4555 Overlook Avenue, SW,Washington,DC,20375**	8. PERFORMING ORGANIZATION REPORT NUMBER
9. SPONSORING/MONITORING AGENCY NAME(S) AND ADDRESS(ES)	10. SPONSOR/MONITOR'S ACRONYM(S)
	11. SPONSOR/MONITOR'S REPORT NUMBER(S)

12. DISTRIBUTION/AVAILABILITY STATEMENT
Approved for public release; distribution unlimited

13. SUPPLEMENTARY NOTES

14. ABSTRACT

15. SUBJECT TERMS

16. SECURITY CLASSIFICATION OF:			17. LIMITATION OF ABSTRACT	18. NUMBER OF PAGES	19a. NAME OF RESPONSIBLE PERSON
a. REPORT **unclassified**	b. ABSTRACT **unclassified**	c. THIS PAGE **unclassified**	**Same as Report (SAR)**	**12**	

lation of the GCR flux. The latitudinal variation of the geomagnetic field imposes a cutoff on the cosmic ray spectrum corresponding to the vertical rigidity cutoff, while the 11-year solar magnetic activity cycle modulates the overall incoming GCR flux in an inverse sense.

[4] Early observations of Earth's γ-ray line spectrum were largely made during balloon flights, which could not achieve wide spatial or temporal coverage. *Ling* [1975] discussed these measurements and presented model source functions for lines independent of time and at fixed latitude. Two satellite missions provided much better coverage, and were much more sensitive than the balloon experiments. These were HEAO 3 during 1979–1980, whose results were reported by *Mahoney et al.* [1981] and *Willett and Mahoney* [1992] (treating the strong 0.511 MeV electron-positron annihilation line, and six strong lines from nuclear interactions, respectively) and the Solar Maximum Mission (SMM), from which results are reported in this paper.

[5] The Gamma Ray Spectrometer experiment (GRS) on board SMM was active during 1980–1989 in LEO and was heavily exposed to Earth atmosphere γ-radiation. It sampled a broad range of the parameters which affected this radiation; its orbital inclination of 28° intercepted geomagnetic cutoff rigidity values between 5–15 GV, and its 10-year lifetime covered the second half of solar cycle 21 and the first half of cycle 22. The HEAO 3 experiment was also in LEO, but at a higher inclination, covering a wider range of cutoff rigidities; it had finer spatial and energy resolution than the GRS, but its lifetime was only 9 months and it was somewhat less sensitive than the GRS.

[6] A spectrum accumulated by SMM during the first $3\frac{1}{2}$ years of the mission at low cutoff rigidities was presented by *Letaw et al.* [1989], and extended to cover the entire mission by *Share and Murphy* [2001], by whom some 20 broad and narrow lines were detected and identified with known lines from high energy impacts upon atmospheric nitrogen and oxygen nuclei. *Share and Murphy* [2001] also detected very broad residual features which could not be so identified. The strong line at 0.511 MeV due to the annihilation of positrons from GCR-induced electromagnetic air showers was also detected. *Letaw et al.* [1989] showed that the time-averaged line strength measurements are in general agreement with the values predicted by *Ling* [1975], and Share and Murphy found agreement with the HEAO 3 measurements also [*Willett and Mahoney*, 1992].

[7] Our purpose here is to follow up this work by measuring the variation of the quiescent Earth atmosphere γ-ray flux with time and latitude. We will use as a surrogate spatial variable the vertical geomagnetic cutoff rigidity, and likewise temporal variability will be expressed in terms of the phase of the solar cycle.

2. Instrument, Observations, and Analysis

2.1. Instrument and Observations

[8] The SMM orbit characteristics were altitude ~400–570 km, inclination 28°, lifetime March 1980–December 1989. It was pointed at the Sun for almost the whole of this time, and therefore observed Earth for an extended period during each ~96-minute orbit. The Earth disk subtended a radius of about 70° at this altitude, which was essentially contained within the GRS's very large field of view (FOV).

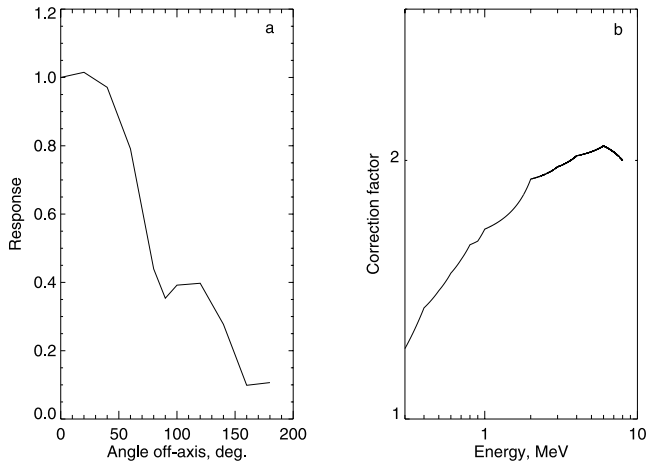

Figure 1. (a) Effective area of the GRS as a function of distance of source off-axis, relative to on-axis (0°), at 1 MeV. (b) Correction factor for the GRS response to a source subtending 68° (as Earth from 500 km altitude) due to leakage of γ-rays through the rear of the detector when pointed away from Earth [*Letaw*, 1988].

The accumulation of data was briefly interrupted (November 1983–April 1984) during preparations for repair of the satellite's attitude control. The instruments were turned off during passages of the South Atlantic Anomaly (SAA) to avoid damage from high radiation doses from trapped particles. Data taken within $\sim 10^4$ s after SAA passages were not used because of intense instrumental background γ-radiation from short-lived radioactivities induced in the SAA. The pattern of SAA passages was strongly influenced by the precession period of the orbit, which was about 48 d.

[9] The spectrometer itself consisted of seven 7.6 × 7.6 cm NaI detectors surrounded to the sides and rear by anticoincidence shielding [*Forrest et al.*, 1980]. It was sensitive to photon energies between 0.3–8.5 MeV, with FWHM resolution ~6% at 1 MeV and binning into 476 energy channels. The energy binning was kept consistent to very good accuracy throughout the mission by active gain control using an on-board ^{60}Co calibration source. The instrument response as a function of energy and angle off-axis was calculated by Monte Carlo simulations (S. Matz, private communication, 1986).

[10] The effective area of the detector at 1 MeV was 120 cm^2. The FOV (~150° at 1 MeV, FWHM, as in Figure 1a) was large enough to contain Earth's disk, as noted above. The spectra were accumulated over 1 min intervals and labeled according to "Earth angle" (i.e., the angle between the Sun pointing and the center of Earth) and geomagnetic cutoff rigidity. They were screened to exclude γ-ray bursts, solar flares and geomagnetic disturbances.

[11] Despite the strength of the Earth atmosphere spectrum, it was dominated in the 1-minute spectra by the background spectrum arising from radioactivity in the GRS and spacecraft induced by energetic particle bombardment, mainly in the SAA [*Share et al.*, 1989]. This may be eliminated by subtracting the count rates in spectra where the FOV points away from Earth from those in spectra pointing towards Earth; the spectra were selected to be within Earth angles 144°–216° and ≤72°, within the same

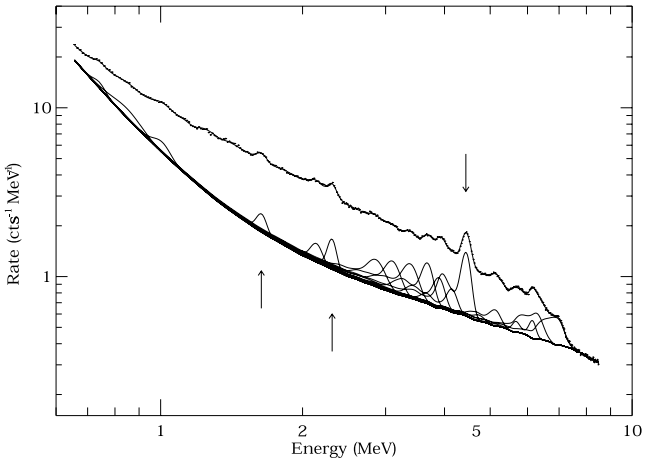

Figure 2. Count spectrum observed by the SMM GRS from Earth's atmosphere accumulated in the geomagnetic cutoff rigidity range 7–9 GV during 1980–1989. Data points, measurements. Thin full lines, the instrument's response to individual lines identified by *Share and Murphy* [2001] superimposed on a two-power-law continuum (lower envelope of lines). Five very broad line-like features of unknown origin are not plotted, either individually or combined with the continuum, for the purpose of clarity (see Figure 11). The sum of all the components as fitted to the measured spectrum is also shown (thick full line). The positions of the important lines at 1.635, 2.311 and 4.44 MeV are shown by arrows.

orbit, and at similar values of cutoff rigidity. The rear shielding of the detector was not sufficient to block Earth radiation completely when pointing away from Earth, especially at high energies, so that when the background subtraction was made the Earth spectrum partially canceled. A correction factor for this effect, as a function of energy, was derived by J. R. Letaw (unpublished report, 1988) from the Monte Carlo simulations mentioned above, and was applied by us to the background-subtracted spectrum (Figure 1b). Otherwise, the background subtraction was very effective, except for two residual lines at the ^{60}Co decay energies 1.17 and 1.33 MeV from the on-board source [*Share and Murphy*, 2001].

[12] After background subtraction the spectra were summed over 3-day intervals. For studies of time and cutoff rigidity dependence the 3-day spectra were summed into several combinations of time and rigidity bins. The basic unit for temporal studies was 48 days, in order to average over any effects arising from background variability on the 48 day precession time-scale. In general the nuclear lines were found to be too weak to be measured with good statistics in 48 days, so we performed a further summation over 6 months for temporal studies. We also made summations over 9 years (i.e., the whole mission) for analyses of cutoff rigidity dependence. The rigidity bins generally employed were <7, 7–11 and >11 GV at 48 d and 6 month resolutions, and <7, 7–9, 9–11, 11–13 and >13 GV over 9 years. There is some contamination of each rigidity bin by its neighbors, due to the GRS's wide FOV, but this can be shown to be small, given the inverse square law of flux and the width of the bins.

[13] A typical spectrum obtained in this way is shown in Figure 2, where the lines identified by *Share and Murphy* [2001] are plotted individually. The unidentified very broad lines detected by *Share and Murphy* [2001] are not plotted in Figure 2.

[14] A systematic uncertainty is expected in this analysis due to γ-ray emission from astronomical sources, in particular the Galactic center (GC). In December of each year Earth's orbital motion causes the apparent position of the Sun to pass very close in angle to the GC, so that for some weeks around this time the GC was almost in the center of the GRS FOV, until the Sun's motion (tracked by the GRS) carried it out of the FOV. This emission was of course only visible when the instrument pointed away from Earth; since these spectra were subtracted from those pointing towards Earth (see above), the peak in emission due to the GC's transit across the FOV ought to appear as a sharp dip in the intensities of the components of our atmospheric spectra around the Decembers of years 1980–1988 [*Share et al.*, 1988]. In practice we found that the dips were detected only in the time series of the narrow 0.511 MeV line, the continuum, and the broad residual features mentioned in section 1, which are so broad that they must be contaminated by the continuum. Results for the 0.511 MeV line from the 6-month and 9-year spectra contained unresolved dips, and were corrected by subtracting the averaged GRS exposure to the dip flux from the GC as a function of time [*Harris et al.*, 1990, Figure 10]. The correction factors were small (∼3%−−5%).

[15] On the shorter 48-day time-scale, the dips are resolved, and are of interest in their own right, since it is possible that an unknown terrestrial source might exist, which exhibits a peak or trough every December. We distinguished between celestial and terrestrial sources of the 0.511 MeV line by looking at our "Earth-viewing" and "sky-viewing" spectra separately on 48 day time-scales. These are both contaminated by lines from radioactive decay, but the 0.511 MeV line from the GC is strong enough to appear in the "sky-viewing" data as positive annual peaks (instead of dips) due to the GC transits [*Share et al.*, 1988, Figure 9]. The "Earth-viewing" spectra should show no signal from the GC (except for a small leakage through the rear of the detector), responding only to terrestrial sources.

2.2. Analysis Procedure

[16] We measured the strengths of the lines in spectra like those of Figure 2 using a model spectrum containing 24 lines and the sum of two power-law continua between the energies 0.65–8.5 MeV. This was identical to the model used by *Share and Murphy* [2001]. The lines were parametrized by energy, width and amplitude; the broad residual features mentioned in section 1 were modeled by 5 broad lines; the continua were parametrized by power law index and amplitude. The model spectra were convolved with the instrument response, with the parameters being varied until the resulting predicted count spectra agreed with the observed spectrum, as specified by the minimum value of the χ^2 function.For fits using such a large number of parameters the minima of the χ^2 function may be shallow and ambiguous. Our method of mapping the function around the minimum is described by *Share and Murphy*

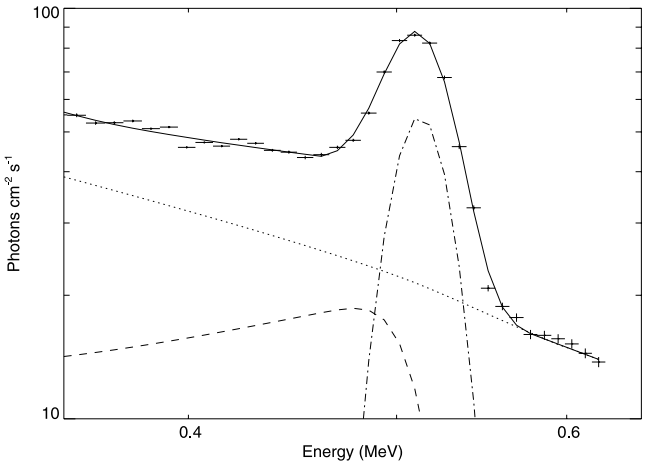

Figure 3. Count spectrum observed by the SMM GRS from Earth's atmosphere accumulated at cutoff rigidities >11 GV during the 48 d interval 6 December 1986 to 19 January 1987, compared with a fitted model spectrum. Data points, measurements; dotted line, power law continuum component; dashed line, Compton scattered component arising from 0.511 MeV line; dot-dashed line, 0.511 MeV line component; full line, sum of three components.

[2001]. In addition to the usual assignment of errors by the criterion of the minimum $\chi^2 + 1$, in some fits systematic errors had to be included to take into account the existence of more than one possible minimum. The model lines were assumed to be of Gaussian shape, and the power laws were constrained so that one dominated the continuum at low energies and the other at high energies.

[17] The positron annihilation line at 0.511 MeV is accompanied by a strong continuum extending to lower energies, resulting from energy losses by Compton scattering in Earth's atmosphere. We performed separate fits to this feature, using a model consisting of a power law continuum between 0.35–0.62 MeV, a narrow line at 0.511 MeV, and a nearly flat continuum extending below 0.511 MeV to account for the scattered component, as illustrated in Figure 3.

3. Results

[18] All of the lines detected by *Share and Murphy* [2001] could be detected in our spectra, though with lower significance due to the cuts we made into time periods and rigidity bins. Both *Willett and Mahoney* [1992] and *Share and Murphy* [2001] have made detailed comparisons between SMM and HEAO 3 measurements. Here we present results for those lines whose temporal or spatial behavior is expected to shed light on physical processes in Earth's atmosphere.

[19] Modelling indicates that the nuclear lines are mainly due to interactions with secondary neutrons produced by GCR impacts, rather than to the GCR themselves [*Ling*, 1975; *Masarik and Beer*, 1999]. We may distinguish between lines produced by de-excitation of excited states of N and O (which are excited by neutrons of ~6–12 MeV), and those produced by de-excitation of spallation products of N and O nuclei, which require higher energies (the cross section rises to a plateau above ~20 MeV). The 4.44 MeV line is the main example of a spallation-product de-excitation (*Ramaty et al.* [1979]—it arises from excited ^{11}B or ^{12}C, which are produced by spallation of ^{14}N and ^{16}O). Most of the other lines result from a combination of spallation and de-excitation processes, as discussed in detail by *Share and Murphy* [2001]. However the two lines at 1.635 and 2.311 in Figure 2 are predominantly the results of de-excitation of ^{14}N. It follows that the ratio of the intensity of the 4.44 MeV to the intensities of the 1.635 and 2.311 MeV lines (combined) is a diagnostic of the relative importance of spallation and de-excitation reactions, and hence of the fluxes of secondary neutrons at high and low energies respectively.

[20] We therefore present our results for, and focus our Discussion on, the three nuclear lines mentioned above and the 0.511 MeV positron annihilation line. We discovered that, as expected, they and the continuum varied at least qualitatively with the solar cycle, being strongest around solar minimum (mid-1986). This is illustrated for the strongest nuclear line in the spectrum, the 4.44 MeV line from de-excitation of ^{12}C and ^{11}B, in Figure 4a. The phase of the solar cycle is illustrated here by the atmospheric neutron fluxes measured at three stations in the global neutron monitor system [*Shea and Smart*, 2000] whose geomagnetic cutoff rigidities correspond approximately to our rigidity bins. The data were obtained from the archive at http://www.env.sci.ibaraki.ac.jp/ftp/pub/WDCCR/STATIONS/. The stations were selected to have comparable altitudes, high count rates [*Moraal et al.*, 2000], and to have been operating during 1980–1989. They are Alma Ata B, Kazakh SSR (rigidity 6.6 GV, altitude 3340 m), Tsumeb, Namibia (rigidity 9.2 GV, altitude 1240 m), and Huancayo, Peru (rigidity 13 GV, altitude 3400 m). We quantify the overall solar-cycle variability as the difference between the

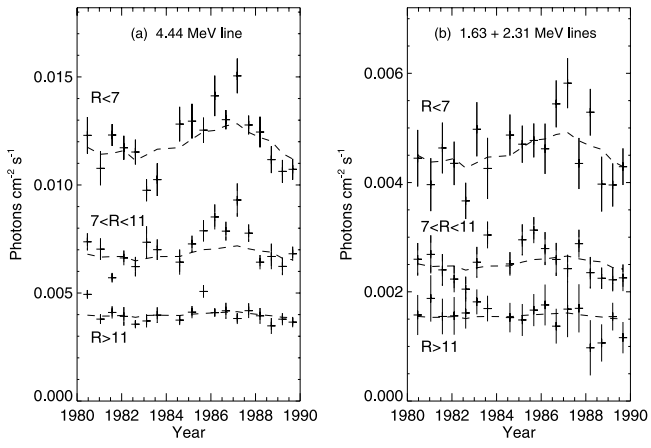

Figure 4. (a) Flux measured in the 4.44 MeV line in six-month periods during 1980–1989 in intervals of geomagnetic cutoff rigidity <7 GV (top), 7–11 GV (middle), >11 GV (bottom). (b) Sums of measurements of the fluxes of the 1.635 and 2.313 MeV lines in the same six-month periods and rigidity intervals. Dashed lines—neutron monitor measurements of atmospheric neutron abundance at Alma Ata B (top), Tsumeb (middle), and Huancayo (bottom) normalized to the line fluxes by simple multiplication (see footnote 2). All fluxes are corrected for detector aperture and efficiency.

Table 1. Comparison of Average Fluxes in Selected γ-Ray Lines During Periods of High and Low Solar Activity as Defined by the Alma Ata B Neutron Monitor

Line or Quantity Averaged	Spectrum (Rigidity)	Interval	Low Activity Average Flux[a] (1980–1983, 1989)	High Activity Average Flux[a] (1984–1988)	Ratio High:Low
4.44 MeV	<7 GV	6 month	11.1 ± 0.2	12.8 ± 0.2	1.16 ± 0.03
	7–11 GV	6 month	6.4 ± 0.1	7.4 ± 0.2	1.14 ± 0.03
	>11 GV	6 month	3.9 ± 0.1	4.1 ± 0.1	1.03 ± 0.03
1.6 + 2.3 MeV	<7 GV	6 month	4.2 ± 0.1	4.9 ± 0.1	1.16 ± 0.05
	7–11 GV	6 month	2.4 ± 0.1	2.6 ± 0.1	1.09 ± 0.05
	>11 GV	6 month	1.6 ± 0.1	1.5 ± 0.1	0.92 ± 0.09
0.511 MeV	<7 GV	48 day	41.3 ± 0.1	45.7 ± 0.1	1.104 ± 0.004
	7–11 GV	48 day	29.9 ± 0.1	31.6 ± 0.1	1.056 ± 0.004
	>11 GV	48 day	23.3 ± 0.1	22.2 ± 0.1	1.051 ± 0.005
Alma Ata B neutrons	6.6 GV	6 month	8709	9385	1.08
Tsumeb neutrons	9.2 GV	6 month	11290	11865	1.05
Huancayo neutrons	13 GV	6 month	1711	1760	1.03

[a]Compare Figures 4 and 5. Gamma-ray line fluxes in units of 10^{-3} photon cm^{-2} s^{-1}. The low and high cosmic ray activity periods were defined by the Alma Ata B count rates being either above or below the mean for the period 1980–1989.

average line fluxes during times of high activity (years 1984 through 1988) and low activity (1980 through 1983, and 1989), which are presented in Table 1.

[21] The figure and table also demonstrate that the 4.44 MeV line intensity falls rapidly as cutoff rigidity increases; again, this is expected due to the shielding from charged particles provided by Earth's magnetic field. The solar-cycle variation amplitude becomes weaker with increasing cutoff rigidity; this is consistent with scaling as the weakening of the flux itself, but in the highest rigidity range (>11 GV) it is also consistent with no variation.

[22] The sum of the intensities of the 1.635 and 2.311 MeV lines is shown as a function of time in Figure 4b. It can be seen that these lines also vary as expected with time (i.e., solar cycle) and cutoff rigidity, as shown quantitatively in Table 1. The temporal behavior of the 0.511 MeV line is also correlated with the solar cycle (Figure 5). In this time series, which is at 48-day resolution, the dips around December due to subtraction of the annual transits of the GC are clearly visible. The dips appear to be larger in the <7 GV cutoff rigidity data, a problem which will be addressed in section 4.3.2. The upper envelope of the time series, if the dips are ignored, agrees qualitatively with the neutron monitor solar cycle proxy. The Compton and power law continua exhibited a second set of strong annual dips due to emission from the Crab Nebula, peaking in June of each year, which made it effectively impossible to discern the shape of the upper envelope of their time series.

[23] To examine the rigidity dependence more fully, we give our results in five rigidity bins from whole-mission spectra in Table 2, for the nuclear lines at 1.635, 2.311 and 4.44 MeV and for the 0.511 MeV annihilation line.

4. Discussion

4.1. Behavior of the Lines From Spallation and Direct De-Excitation

[24] As noted in section 3, the ratio of the intensities of the lines at 4.44 MeV and 1.635 plus 2.311 MeV is a function of the relative importance of spallation reactions and nuclear de-excitations caused by impacts of neutrons on atmospheric nuclei. This in turn depends on the relative fluxes of secondary neutrons below 12 MeV and above 50 MeV respectively, due to the energy dependence of the cross sections, which we consider below. In Figure 6, using the measurements in Figure 4, we plot the ratio between the strengths of the 1.635 plus 2.311 MeV lines and the 4.44 MeV line from 1980 to 1989. It is found to be essentially constant at all times and in all cutoff rigidity bins—in the figure, variability of the points within each panel is not significant, nor are the differences between the long-term averages of each panel. The same result is also obtained from the results integrated over 9 years for the finer rigidity binning in Table 2—the fluxes in both categories of line fall as cutoff rigidity increases, approximately in lockstep at a rate ∼15% per GV of rigidity.

[25] We will compare these measured ratios of 1.635 plus 2.311 MeV to 4.44 MeV lines with theoretical predictions. We generated the predictions from a neutron spectrum above 1 MeV at the top of the atmosphere (30 g cm^{-2}) at

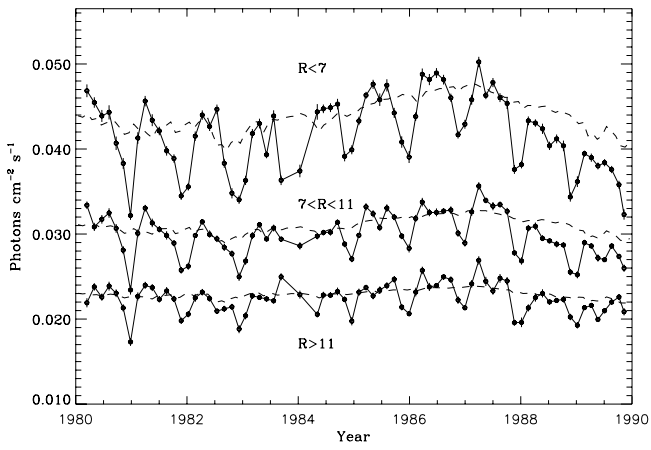

Figure 5. Data points, flux measured in the 0.511 MeV line in 48-day periods during 1980–1989 in intervals of geomagnetic cutoff rigidity <7 GV (top), 9–11 GV (middle), >13 GV (bottom). Full lines, neutron monitor measurements from Alma Ata B (top), Tsumeb (middle) and Huancayo (bottom), normalized to the line fluxes by simple multiplication (see footnote 2). All fluxes are corrected for detector aperture and efficiency.

Table 2. Fluxes in Selected γ-Ray Lines During the Entire Mission 1980–1989 as a Function of Geomagnetic Vertical Cutoff Rigidity, Normalized to Rigidity <7 GV

Rigidity Cutoff GV	Live Time Seconds	Sum Flux 1.635 MeV + 2.311 MeV	Flux 4.44 MeV	Flux[a] 0.511 MeV	Downward Cosmic Ray Proton Flux
<7	3.64×10^6	1[b]	1[c]	1[d]	1[e]
7–9	2.95×10^6	0.66 ± 0.04	0.73 ± 0.02	0.805 ± 0.007	0.606
9–11	4.08×10^6	0.51 ± 0.04	0.49 ± 0.01	0.624 ± 0.005	0.444
11–13	5.89×10^6	0.34 ± 0.02	0.37 ± 0.01	0.532 ± 0.005	0.348
>13	1.25×10^6	0.27 ± 0.03	0.28 ± 0.01	0.479 ± 0.005	0.321

[a]Corrected for contamination by the GC 0.511 MeV line source as described in the text, section 2.1.
[b]Value before normalization: $4.5 \pm 0.1 \times 10^{-3}$ photon cm^{-2} s^{-1}.
[c]Value before normalization: $1.19 \pm 0.02 \times 10^{-2}$ photon cm^{-2} s^{-1}.
[d]Value before normalization: $4.38 \pm 0.03 \times 10^{-2}$ photon cm^{-2} s^{-1}.
[e]Value before normalization: 412.7 proton m^{-2} s^{-1} sr^{-1}.

high rigidity (15 GV) calculated by *Kollar and Masarik* [1999] using Monte Carlo simulation. We approximated this neutron spectrum by a broken power law

$$0.07E^{-1.29} \text{ neutrons}/(\text{cm}^2 \text{ s MeV}) \quad \text{for } E \le 10^4 \text{ MeV}$$
$$2.6 \times 10^3 E^{-2.31} \text{ neutrons}/(\text{cm}^2 \text{ s MeV}) \quad \text{for } E > 10^4 \text{ MeV} \quad (1)$$

[26] We used the standard reaction rate formula [*Lang*, 1980] in which this distribution is folded with the cross sections for neutron inelastic scattering and spallation on ^{14}N. These are available below 20 MeV from *Rogers et al.* [1975] — above 20 MeV the inelastic cross sections go to zero and the spallation cross section can be assumed to be constant at its value 40 ± 8 mb at 20 MeV. The 20% uncertainty in the ^{14}N spallation cross section producing 4.44 MeV photons is the major source of systematic error in this calculation. Taking it into account, we computed a predicted ratio of $0.36^{-0.06}_{+0.08}$, in very good agreement with our measurement of 0.39 ± 0.03 at high rigidity >11 GV (Table 1 and Figure 6, right panel).

[27] We now quantify the extent to which the shape of this neutron spectrum is allowed to vary, given that our result is consistent with a shape varying neither with time nor with cutoff rigidity (Figure 6). For this purpose we take the low-energy power law index in equation (1) as the parameter of interest, since the high-energy power law contributes little. We repeated our calculation of the (1.635 + 2.311 MeV)/4.44 MeV ratio with this index allowed to vary, for ^{14}N spallation cross section values in the allowed range 32–48 mb. The power law index was allowed to vary until the 3σ limits on the variation of the line ratio from high to low phase of the solar cycle were exceeded (i.e., 0.39 ± 0.09 at high cutoff rigidity >11 GV). Figure 7 shows the results (left panel). The dotted line represents the power law index which reproduces the mean

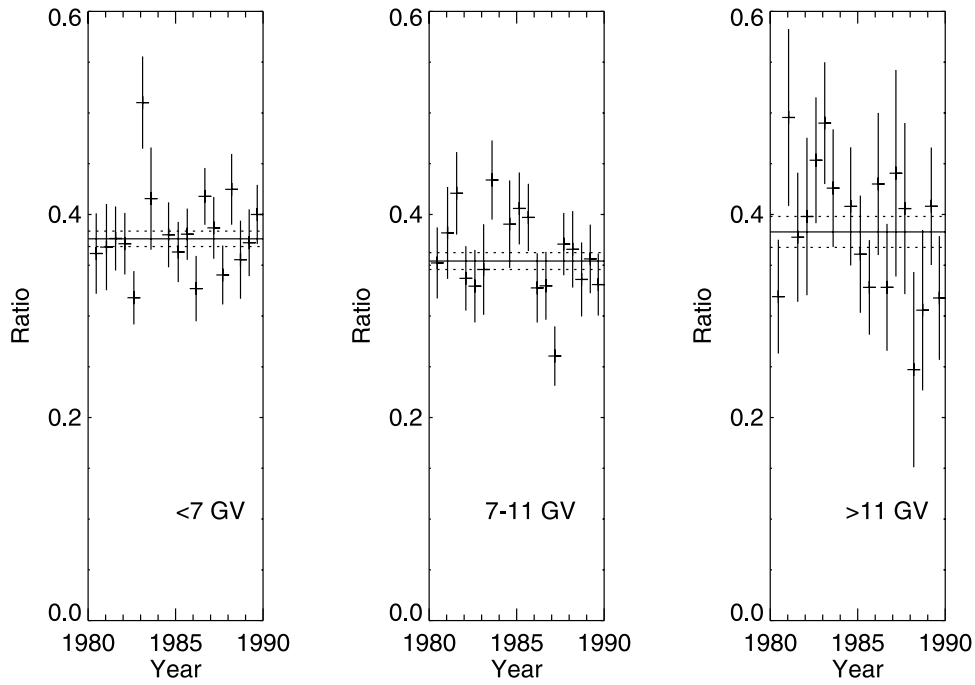

Figure 6. Data points, ratio of the sum of the six-monthly 1.635 and 2.313 MeV line strengths to that of the 4.44 MeV line (see Figure 4) for cutoff rigidity intervals <7 GV (*left*), 7–11 GV (*center*), and >11 GV (*right*). Full lines, mean value of the ratio during the mission for each rigidity interval. Dash lines, 1σ errors on the mean values.

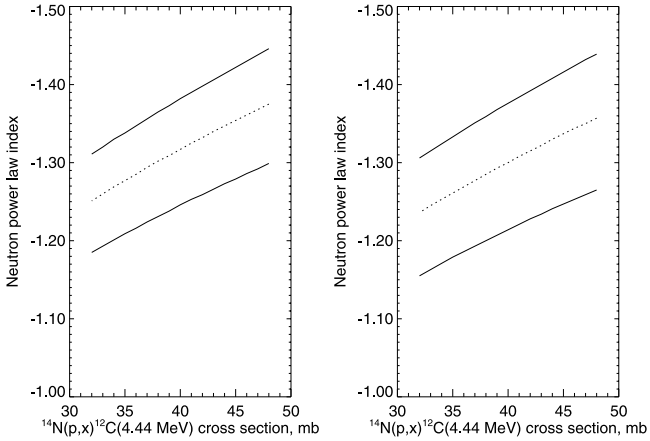

Figure 7. Allowed range of variability of the energy spectrum of atmospheric neutrons at 30 g cm^{-2} depth, in the approximation of two power laws in energy broken at 10^4 MeV. Variability is parametrized by the values of the low energy power law index permitted by *SMM*'s measured limits on the γ-ray line ratio (1.6 + 2.3)/4.4 MeV in Figure 6. The effect of the experimental uncertainty in the ^{14}N(p, x)^{12}C*(4.44 MeV) cross section at 20 MeV is shown (abscissa). (left) Variability in time allowed by the SMM measurement of the line ratio at rigidities >11 GV 0.39 ± 0.03 (see Figure 6 right panel). (right)—variability with cutoff rigidity allowed by the SMM measurement 0.37 ± 0.03 (from range of mean values of all three panels in Figure 6). In both panels the dotted line is the power law index which reproduces the measured line ratio for a given ^{14}N + p cross section and the solid lines are the limits which are consistent with that ratio at 3σ.

line ratio 0.39 as a function of the spallation cross section and the full lines are the 3σ limits. It is clear that, while the absolute value of the power law index may lie anywhere within the range ∼−1.2−−1.45, for a given ^{14}N spallation cross section it can only vary from the central value by about 5% over time.

[28] We next consider the allowable variation of the neutron spectral shape with cutoff rigidity. A further assumption about the shape is necessary here, since predictions at cutoff rigidities in the 5–11 GV range were not published by *Masarik and Beer* [1999] and *Kollar and Masarik* [1999]; predictions were published for high magnetic latitudes (>70° and gave a neutron spectrum shape similar to that at the equator. We therefore make the very simple assumption that the neutron energy spectrum at any rigidity has the same broken power law shape as in equation (1) such that the amplitudes of the two terms are multiplied by a common constant factor. The calculation of the predicted (1.635 + 2.311 MeV)/4.44 MeV line ratio as a function of the low-energy power law index and the ^{14}N spallation cross section proceeded exactly as described above for the time variability limits. Our limit for the allowed variability of this ratio as a function of cutoff rigidity was found from Table 2 to be 0.37 ± 0.03 (1σ), or 0.37 ± 0.09 (3σ). As would be expected from the constancy of this ratio with both time and rigidity, the resulting limits on the power law index are almost the same for spatial as for temporal variability (Figure 7, right): the absolute value may lie between ∼−1.15−−1.45, but for any given ^{14}N spallation cross section it can only vary by about ±6% between rigidities 5–15 GV.

[29] In summary, despite the presence of a systematic uncertainty in its value due to the experimental error in the nuclear cross sections, the variability of the neutron spectrum's low-energy power law index with time and cutoff rigidity is tightly constrained—whatever the actual value of the index may be, the allowed changes during a solar cycle, and over the range of cutoff rigidities 5–15 GV, are ≤5%−6% (3σ).

4.2. Amplitude of Solar-Cycle Modulation

[30] It is quite clear from Figures 4a and 4b that in general the nuclear γ-ray line fluxes are more strongly modulated than the count rates from ground-based neutron monitors which were selected to have similar geomagnetic cutoff rigidities. This is shown quantitatively in Table 1 where we compare, for both the γ-ray lines and the neutron monitors, the fluxes during low and high cosmic ray activity periods.

[31] At first sight this is unexpected, since the same incident cosmic ray spectra are producing the neutrons which are responsible for both measurements. There is, however, an effect predicted by theoretical simulations of the neutron fluxes in the atmosphere, as a function of depth, which can explain this result. The key physical process is that that at the top of the atmosphere neutrons are able to escape upwards, and this leakage probability depends on the cosmic ray proton energy spectrum; lower energy protons are more likely to generate upward-leaking neutrons. Spacecraft of course see the effects of both upward and downward moving neutrons, whereas ground based measurements see only the latter. The effect is illustrated in Figure 8 [after *Light et al.*, 1973]. Note that our results in section 4.1 require that the shape of the neutron spectrum is practically independent of the hardness of the proton spectrum — it is the direction of the neutrons (up or down) which is affected. This is illustrated in Figure 8, where changes in the proton energy have a very similar effect on neutrons both above

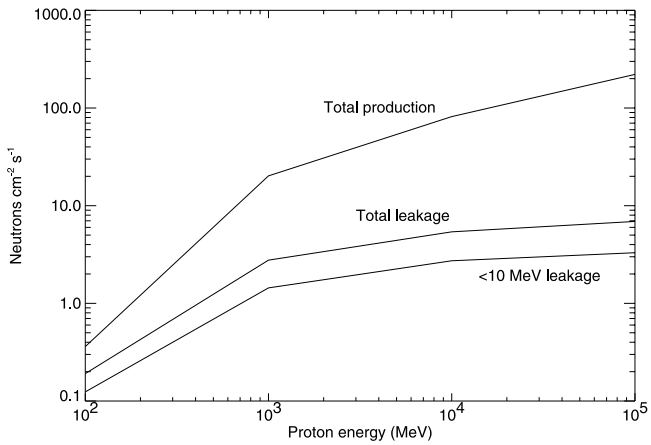

Figure 8. Column-integrated rates of neutron production by monoenergetic protons incident at the top of the atmosphere, and of neutron upward leakage, computed by *Light et al.* [1973]. The fraction of leakage neutrons below 10 MeV is also shown.

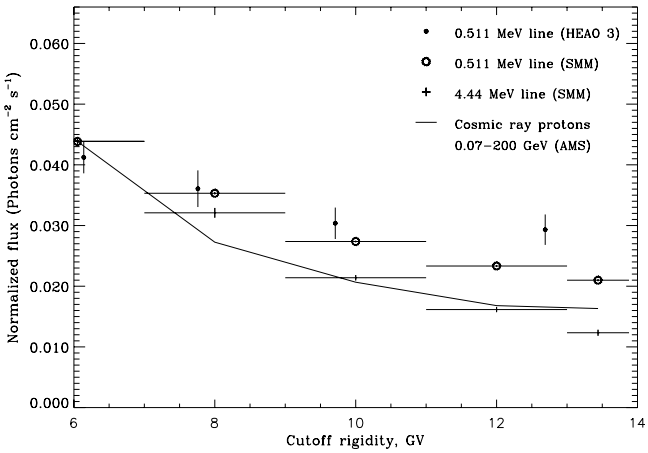

Figure 9. Intensities of the 0.511 MeV line (open circles) and the 4.4 MeV line (crosses) measured from spectra accumulated in five geomagnetic cutoff rigidity intervals during the entire mission (Table 2). Filled circles—intensities of the 0.511 MeV line measured by the HEAO-3 spectrometer [*Mahoney et al.*, 1981]. Full line, downward flux of cosmic ray protons with energies between 0.07–200 GeV measured by AMS. The 4.4 MeV and proton fluxes are normalized to agree with the SMM 0.511 MeV line flux for rigidities <7 GV (Table 2, footnote d). The HEAO-3 measurements are corrected to account for the GRS FOV and for limb darkening as described in the text.

and below 10 MeV, (i.e., those causing both de-excitation lines and spallation lines). This is consistent with the leakage neutron spectrum remaining approximately unchanged even when the incident proton spectrum changes substantially, as required by our results in section 4.1.

[32] A direct test of this solar modulation effect cannot be made, since no detailed simulations have been published for the neutron spectrum as a function of solar cycle phase and atmospheric depth. However simulations as a function of cutoff rigidity and depth were performed by *Kollar and Masarik* [1999], and the effect of high rigidity is qualitatively similar to that of strong solar modulation, i.e., a hardening of the incoming proton spectrum. In these simulations the total neutron flux falls off much faster between the top and bottom of the atmosphere at low rigidities than at high rigidities. Thus the neutron flux at a depth ~20 g cm^{-2} (as seen from orbit) falls by a factor of 10 between cutoff rigidities 0.2 GV and 15 GV, while the neutron flux at the mountain-top level of the neutron monitors falls only by a factor 2. The harder proton energy spectrum at 15 GV produces neutrons less likely to escape, and therefore relatively more likely to reach 1000–3000 m.

[33] This effect must also occur when changes in the proton energy spectrum arise from the solar cycle modulation rather than from varying geomagnetic cutoff rigidity. Thus the reduced amplitude of the modulation of the neutron monitor count rates relative to our line flux measurements is due to the softer cosmic ray spectrum around solar minimum giving rise to relatively enhanced leakage of neutrons which are visible to spacecraft but not to ground-based instruments. The softening of the spectrum is however much less pronounced between the extremes of a solar cycle than between cutoff rigidities 0.2–15 GV, so that the differences up to ~8% between the modulations at the top and bottom of the atmosphere (Table 1) due to the solar cycle are much less than the factor of 5 which the models predict to result from varying geomagnetic cutoff rigidity.

4.3. The 0.511 MeV Electron-Positron Annihilation Line

4.3.1. Comparison With the Nuclear De-excitation and Spallation Lines

[34] The atmospheric 0.511 MeV positron annihilation line owes its existence to pair production from the energetic photons generated in the electromagnetic component of air showers produced by very energetic GCR, not to secondary neutrons. Although its intensity falls off with increasing cutoff rigidity R, Figure 9 (based on Table 2) clearly show that it falls less rapidly than the intensity of the 4.44 MeV line. The 4.44 MeV and other nuclear lines fall by factors of almost 4 when cutoff rigidity increases from <7 GV to >13 GV, while the 0.511 MeV line falls off only by a factor ~2.

[35] Some insight into the energy dependence of these primary processes can be gained by comparing the dependence on R of the lines with the rate of fall-off of the downward cosmic ray proton flux with R, which was measured by the Alpha Magnetic Spectrometer (AMS) experiment [*Alcaraz et al.*, 2000] and is also plotted in Figure 9. The AMS measurements covered proton energies E_p in the range 70 MeV–200 GeV. It is seen that the 4.44 MeV line flux falls off approximately in step with the cosmic ray proton flux, whereas the 0.511 MeV line quite clearly falls less steeply with increasing R. The behavior of the 4.44 MeV line implies that the multiplicity of the secondary neutrons which generate the 4.44 MeV line is not a strong function of E_p. As noted in section 4.1, models suggest that the shape of the secondary neutron spectrum is much less variable with cutoff rigidity than the cosmic ray proton spectrum [*Kollar and Masarik*, 1999]. The R-dependence of the 4.44 MeV line might nevertheless differ from that of the proton flux if the multiplicity of neutrons produced per proton is a strong function of E_p. The similarity between the curves for cosmic ray protons and the 4.44 MeV line in Figure 9 suggests that this is not the case. Model calculations of neutron production by nuclear evaporation predict a neutron multiplicity $\sim E_p^{0.2}$ for N and O [*Konecná et al.*, 1999], confirming that it is indeed a weak function of proton energy.

[36] A second implication of the curves in Figure 9 is that, conversely, the air shower process which generates positrons and then 0.511 MeV photons is a strong function of energy—the decreasing number of cosmic ray protons as R increases must be partly offset by the fact that the remaining protons are more energetic and more efficient at producing positrons. The electromagnetic cascade is produced by the "soft" component of a charged particle induced shower. Charged particle strong interactions produce a shower of pions which may undergo further strong interactions (producing the "hard" component of the air shower), or decay into energetic γ-rays or leptons; electron-positron pair production by electromagnetic interactions of these particles is well understood [*Lang*, 1980]. The multiplicity of secondary pions at these energies is a rather weak

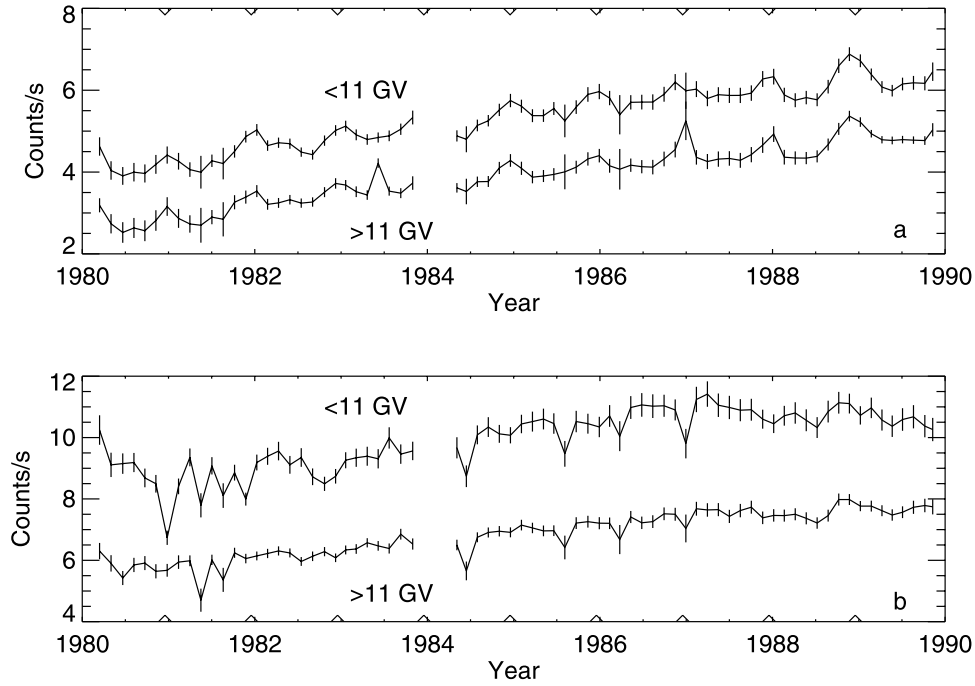

Figure 10. (a) Flux measured in the 0.511 MeV line in 48-day periods at cutoff rigidities >11 GV and <11 GV when the GRS was pointed away from Earth ("sky-viewing"; Earth angles 144°−−216°). Note the long-term trend due to buildup of β^+-emitting radioactivities, with annual peaks superimposed due to transits of the GC across the aperture. (b) Flux measured in the 0.511 MeV line in 48-day periods at cutoff rigidities >11 GV and <11 GV when the GRS was pointed towards Earth (Earth angles <72°). Carets show the epochs of GC transits.

function of energy, varying as $E_p^{0.3}$: [*Wigmans*, 2003]), but the cross section for pair production increases rapidly, as $\sim \ln^3(E_p)$, confirming our expectation. The relative R-dependences of the 4.44 and 0.511 MeV lines in Figure 9 are therefore qualitatively explained by the E_p-dependences of the multiplicities with which secondary particles (neutrons or pions) are produced, and of the cross sections of the reactions which follow.

4.3.2. Anomalous Rigidity Dependence of the Galactic 0.511 MeV Line

[37] The annual dips in the time series of 0.511 MeV line fluxes, which are clearly visible in Figure 5, are apparently dependent upon R: the dips in the bin <7 GV cutoff rigidity are about twice as deep as those in the other bins. This is not expected from the theory of GC transits developed by *Share et al.* [1988] since (given the constant GC source) the dip amplitude depends only on the occultation geometry, which is not expected to vary significantly with rigidity. There are three possible causes: selection effects in the transit geometry at low rigidity, the transiting of a second, unknown cosmic 0.511 MeV line source across the GRS FOV, or an unexpected effect intrinsic to the LEO environment which happens to cause a drop in the atmospheric 0.511 MeV line flux every December.

[38] We tested for the presence of a cosmic or terrestrial source of the dips by dividing our spectra into "Earth-viewing" and "sky-viewing" periods as described in section 2.1; the dips in a time series of "Earth-viewing minus sky-viewing" 0.511 MeV amplitudes should appear as peaks in the "sky-viewing" subset, and not at all in the "Earth-viewing" subset. The R dependence of the dips in Figure 5 might be caused by a rigidity dependence of the "sky-viewing" peaks (as in the first two hypotheses above) or by rigidity-dependent dips in the "Earth-viewing" subset (as in the third hypothesis). We fitted 48-day accumulated spectra of each type between 0.35−0.75 MeV (subdivided into subsets with $R > 11$ and $R < 11$) with a model spectrum containing four known lines from spacecraft radioactvity and the 0.511 MeV, plus a power law continuum (there is a full description in *Share et al.* [1988]). The resulting amplitudes for the 0.511 MeV line are shown in Figures 10a and 10b. It is clear that the annual "sky-viewing" peaks are not significantly dependent upon R. The "Earth-viewing" spectra, by contrast, show dips which are much stronger at low rigidity. However, the relation between these dips and December of the calendar is not very strong.

[39] This analysis shows that the effect is terrestrial in origin.We confirmed that the source is not celestial by calculating the exposures of the GRS to the GC and other possible cosmic sources when in the $R < 7$ and $R > 11$ GV portions of the orbit [cf. *Share et al.*, 1988; *Harris et al.*, 1990]. We found no significant differences. The apparent strengthening of the GC-induced dips in December in Figure 5 appears to be a chance occurrence of a small number of R-dependent dips at that time of year (Figure 10b).

[40] There is no immediately obvious candidate for an effect intrinsic to Earth's atmosphere which is restricted to low geomagnetic cutoff rigidities and operates sporadically on a 48-day time-scale. The dips do not appear to be more

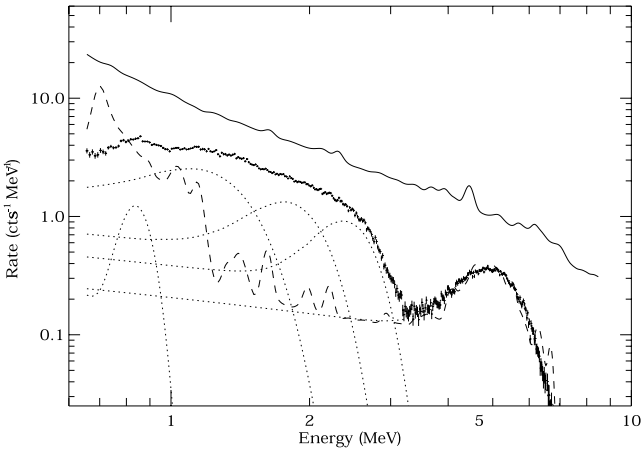

Figure 11. The count spectrum of Figure 2 with the continuum and narrow lines subtracted. Data points, the residual spectrum after the subtraction. Full line, the fitted sum of all spectral features as in Figure 2. Dotted lines, five broad line-like features not shown in Figure 2, which fit the residual spectrum. Dashed line, the response of the SMM GRS to the line spectrum from thermal neutron capture on iodine, normalized to agree with the broad feature at 5 MeV.

frequent at any phase of the solar cycle, or to correlate with geomagnetic events. Equally, an artefact of unknown origin in the instrument or in our analysis may be responsible.

4.3.3. Comparison With HEAO 3 Results

[41] The 0.511 MeV annihilation line was strong enough for the HEAO 3 count rates at this energy to be broken down into bins of geomagnetic cutoff rigidity, much as we have done (section 2.1). We compare our result (Table 2) with that of *Mahoney et al.* [1981] in Figure 9 (open versus closed circles). The HEAO 3 flux values per steradian have been integrated over the *SMM* exposure to the 68° Earth disk. This integration was also weighted by the limb darkening function which *Mahoney et al.* [1981] measured using HEAO 3's superior spatial resolution, which is proportional to $1 + 1.7 \cos \theta$ where θ is the satellite zenith angle seen from a disk point. The HEAO 3 measurements then agree well with the SMM values, though having a rather shallower decrease with cutoff rigidity. They are consistent with our finding that the 0.511 MeV line falls off more slowly with rigidity than the 4.44 MeV line, and with our explanation in terms of the interaction cross sections involved (section 4.2).

4.4. Broad Residual Lines at 1– 5 MeV

[42] We noted in Figure 2 that, in addition to the narrow lines shown there, five broad lines were necessary to fit the spectrum [*Share and Murphy*, 2001]. The actual residual features which are fitted by these five lines are shown in Figure 11. The peak around 5 MeV suggested to *Share and Murphy* [2001] that thermal or epithermal neutron capture on the ^{127}I in the NaI and CsI detectors was responsible. We repeated their comparison between the I thermal neutron γ-ray spectrum and the residual features using an updated database of I lines. Figure 11 shows that the agreement is worse than that found by *Share and Murphy* [2001], although the discrepancy at energies <1 MeV when normalized to the 5 MeV feature is only a factor ∼2.

[43] Our result in Figure 11 suggests that the residual feature in the 1–3 MeV range is due mainly to a different process from the instrumental neutron captures which generate the ∼5 MeV peak. We propose that there are atmospheric nuclear lines in this range which are not resolved by the GRS. Additional evidence for this comes from the dependences of the strengths of the 1–3 and 5 MeV residual features on geomagnetic cutoff rigidity in the range $R \leq 13$ GV (Figure 12). In section 4.1 we noted that atmospheric nuclear lines in general decrease at approximately the same rate when rigidity increases—the characteristic behavior, taking the 4.44 line as typical, is a decrease in strength by about 15% per GV (Table 2). The broad 1–3 MeV residual feature shares this behavior: the ratio between this feature and the 4.44 MeV line is plotted in Figure 12 and seen to be approximately constant below 13 GV—there is clearly some other process at work above 13 GV (see below). The constancy below 13 GV is consistent with the feature being composed of unresolved atmospheric lines from nuclear spallation reactions or nuclear de-excitation (the underlying reason being the constancy of the secondary neutron spectrum, section 4.1).

[44] Compared with the 15% per GV rigidity fall-off rate of both the atmospheric nuclear lines and the 1–3 MeV feature, the 5 MeV residual feature in Figure 12 falls off much faster for $R \leq 13$ GV. This is expected if it arises from thermal or epithermal neutron captures in orbit, i.e., the upward leakage neutrons whose behavior was discussed in section 4.2. In our comparison of neutron monitor and satellite data we found that as R increases the primary GCR proton spectrum becomes much harder, whereas upward-leaking neutrons are more efficiently produced by low energy protons (Figure 8). Just as relatively more neutrons reach ground-based neutron monitors at high R, relatively fewer neutrons will reach LEO—i.e., the ratio between LEO neutrons and atmospheric neutrons gets smaller as rigidity increases, as does the ratio between the 1–3 MeV and ∼5 MeV features in Figure 12 below 13 GV.

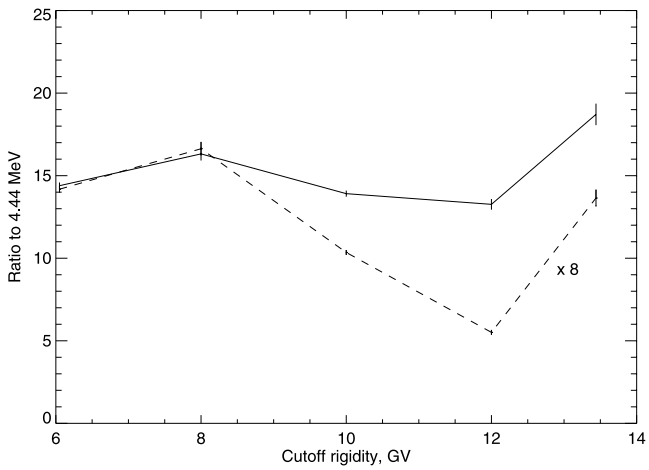

Figure 12. Ratio of the count rates in the broad features 1–3 MeV (full line) and 5 MeV (dashed line) to the strength of the 4.44 MeV line as a function of cutoff rigidity. The lower bound of the 5 MeV feature is assumed to be 3.8 MeV, and its ratio to 4.44 MeV is multiplied by 8 for clarity.

[45] It is clear from Figure 12 that at the highest rigidities $R > 13$ GV (close to the geomagnetic equator) there is a different process acting. The 5 MeV residual feature rises sharply, and the 1–3 MeV residual feature shows a less marked increase, relative to the 4.4 MeV line. We suggest that these increases result from the same epithermal neutron captures on I, but that there is a distinct equatorial population of neutrons over and above the up-going neutrons produced directly by GCR (whose abundance is lowest at the equator). One possible source of such neutrons is the LAP (low altitude particles) detected at energies above 500 keV by *Hovestadt et al.* [1972] at low geomagnetic latitudes. These ions are ultimately derived from the equatorial ring current, but extend much lower in altitude (down to <100 km). Their abundance depends only weakly on solar activity [*Mazur et al.*, 1998]. Their energy spectrum extends at least up to 35 MeV [*Gusev et al.*, 1996], well above the ~6 MeV thresholds of the reactions $^{14}N(p, n)^{14}O$ and $^{14}N(\alpha, n)^{17}F$. Neutrons produced in this way would have low (epithermal) energies, as required for the 5 MeV residual feature, making a small contribution to the 1–3 MeV feature also (Figure 11, dashed line). A weak point of this hypothesis is that the spectrum measured by *Mizera and Blake* [1973] and *Gusev et al.* [1996] is very soft (varying as energy $E^{-4.4}$ if a power law), so that relatively few ions exceed the reaction thresholds.

[46] Alternatively, albedo charged particles (electrons [*Basilova et al.*, 1979], protons [*Efimov et al.*, 1985], referred to by *Alcaraz et al.* [2000] as the "second spectrum") are known to rise in numbers near the geomagnetic equator. Unlike the albedo neutron population, their fluxes are not related in a simple way to the primary GCR fluxes, due to their very complex trajectories in the geomagnetic field. Like the neutrons, they are thought to originate in GCR impacts on atmospheric nuclei. The albedo protons have moderately hard spectra extending up to a few GeV and thus occur above the threshold energy for neutron production. A drawback to this model is the uncertainty in the propagation of the particles in the magnetic field, which was derived by *Alcaraz et al.* [2000] from Monte Carlo simulations rather than observation. The simulations suggest that only a subset of albedo protons—those whose trajectories involve many mirrorings over a relatively long lifetime ("quasi-trapped")—are equatorially concentrated, and it is suggested that their origin is associated with the energetic trapped SAA particles. The flux is not expected to be isotropic, having a strong east-west gradient, which makes the directionality of any resultant neutrons, and SMM's response to them, very difficult to predict. The properties of these particles are reviewed by *Huang* [2001].

5. Summary

[47] We suggest four conclusions as to the behavior of the atmospheric γ-ray lines which we have studied here.

[48] 1. The temporal behavior of all lines can be explained by the varying modulation of the incident GCR flux during the solar cycle.

[49] 2. The lines produced by two processes arising from secondary neutrons (spallation and de-excitation of air nuclei) behave similarly with respect to geomagnetic location (i.e., cutoff rigidity).

[50] 3. It follows from this that the shape of the secondary neutron energy spectrum is not strongly variable over the solar cycle or over the limited range of cutoff rigidities sampled by SMM. If we assume a simplified broken power-law spectrum of secondary neutrons, then the low energy power law index must lie in the approximate range −1.15–−1.45. There is a systematic error in the absolute value, but the variability in that absolute value over a solar cycle must be <5%; the spatial variability over the cutoff rigidity range 5–15 GV must likewise be <6% (both 3σ upper limits).

[51] 4. The behaviors of these neutron-induced lines and of the 0.511 MeV positron annihilation line with respect to cutoff rigidity are different, and the difference can be explained by the rigidity dependence of the measured GCR proton flux and by the cross sections for the elementary particle interactions which produce them (respectively, secondary neutron production, and electromagnetic cascades from energetic secondary pions).

[52] We find that the signal from the known Galactic 0.511 MeV line (superposed on that from Earth's atmosphere) unexpectedly shows a dependence on cutoff rigidity (section 4.3.2), which appears to be due to the infrequent chance occurrence of unexplained short decreases in the Earth-atmosphere 0.511 MeV line signal at higher latitudes.

[53] The origins of two very broad residual features in the spectrum (~1–3 MeV and 5 MeV, which we modeled by five broad Gaussian lines) appear to be complex. We tentatively suggest that most of the 1–3 MeV feature comes from the contribution of many weak unresolved atmospheric lines, while the rest of the 1–3 MeV feature and the whole of the 5 MeV feature are due to the capture of ambient thermal or epithermal neutrons in the iodine in the GRS detectors. If true, this requires the existence of two distinct populations of neutrons in LEO, one of which follows the cutoff rigidity law described above (second and third conclusions) while the other is confined to low geomagnetic latitudes.

[54] **Acknowledgments.** We are grateful to Ben-Zion Kozlovsky of Tel Aviv University and Ron Murphy of NRL for helpful discussions, and to two referees for their suggested improvements. This work was supported by NASA grant DPR W19916.

[55] The Editor thanks Juan Alcaraz and another referee for their assistance in evaluating this paper.

References

Alcaraz, J., et al., Protons in near Earth orbit, *Phys. Lett. B*, *472*, 215–226, 2000.

Basilova, R. N., E. I. Kogan-Laskina, G. I. Pugacheva, and I. A. Savenko, The quasi-trapped electron flux with E > 80 MeV at an altitude of 200–250 km, *Proc. Int. Conf. Cosmic Ray 16th*, *3*, 150–153, 1979.

Efimov, Y. E., A. A. Gusev, K. Kudela, L. Just, and G. I. Pugacheva, Spatial distribution of albedo particles on altitudes ~500 km, *Czechoslovak J. Phys.*, *B35*, 1371–1381, 1985.

Forrest, D. J., et al., The gamma ray spectrometer for the Solar Maximum Mission, *Solar Phys.*, *65*, 15–23, 1980.

Gusev, A. A., T. Kohno, W. N. Spjeldvik, I. M. Martin, G. I. Pugacheva, and A. Turtelli Jr., Dynamics of the low-altitude energetic proton fluxes beneath the main terrestrial radiation belts, *J. Geophys. Res.*, *101*, 19,659–19,663, 1996.

Harris, M. J., G. H. Share, M. D. Leising, R. L. Kinzer, and D. C. Messina, Measurement of the 0.3–8.5 MeV Galactic gamma-ray spectrum from the Galactic center direction, *Astrophys. J.*, *362*, 135–146, 1990.

Hovestadt, D., B. Häusler, and M. Scholer, Observation of energetic particles at very low altitudes near the geomagnetic equator, *Phys. Rev. Lett.*, *28*, 1340–1344, 1972.

Huang, M. A., Physics results from the Alpha Magnetic Spectrometer 1998 Shuttle flight, in *Proceedings of 7th Taiwan Astrophysics Workshop*, edited by C.-M. Ko, World Sci., Singapore, 2001.

Kollar, D., and J. Masarik, Numerical simulation of particle fluxes and cosmogenic nuclide production rates in Earth atmosphere, *Acta Phys. Univ. Comenianae*, *40*, 81–93, 1999. (Available at http://javier.dnp.fmph.uniba.sk/~dkollar/work/acta1999.pdf, 1999)

Konecna, Á., V. Valenta, and V. Smutný, Calculations of spallation neutrons yields from targets, paper presented at Third International Conference on ADTT and Applications, Prague, 1999.

Lang, K. R., *Astrophysical Formulae*, Springer-Verlag, New York, 1980.

Letaw, J. R., G. H. Share, R. L. Kinzer, R. Silberberg, E. L. Chupp, D. J. Forrest, and E. Rieger, Satellite obsevations of atmospheric nuclear gamma radiation, *J. Geophys. Res.*, *94*, 1211–1221, 1989.

Light, E. S., M. Merker, H. J. Verschell, R. B. Mendell, and S. A. Korff, Time dependent worldwide distribution of atmospheric neutrons and of their products, *J. Geophys. Res.*, *78*, 2741–2762, 1973.

Ling, J. C., A semiempirical model for atmospheric γ rays from 0.3 to 10 MeV at $\lambda = 40°$, *J. Geophys. Res.*, *80*, 3241–3252, 1975.

Mahoney, W. A., J. C. Ling, and A. S. Jacobson, HEAO 3 measurements of the atmospheric positron annihilation line, *J. Geophys. Res.*, *86*, 11,098–11,104, 1981.

Masarik, J., and J. Beer, Simulation of particle fluxes and cosmogenic nuclide production in the Earth's atmosphere, *J. Geophys. Res.*, *104*, 12,099–12,111, 1999.

Mazur, J. E., G. M. Mason, and M. E. Greenspan, The elemental composition of low altitude 0.49 MeV/nucleon trapped equatorial ions, *Geophys. Res. Lett.*, *25*, 849–852, 1998.

Mizera, P. F., and J. B. Blake, Observations of ring current protons at low altitudes, *J. Geophys. Res.*, *78*, 1058–1062, 1973.

Moraal, H., A. Belov, and J. M. Clem, Design and co-ordination of multi-station international neutron monitor networks, *Space Sci. Rev.*, *93*, 285–303, 2000.

Ramaty, R., B. Kozlovsky, and R. E. Lingenfelter, Nuclear gamma-rays from energetic particle interactions, *Astrophys. J. Suppl. Ser.*, *40*, 487–526, 1979.

Rogers, V. C., V. J. Orphan, C. G. Hoot, and V. V. Verbinski, Gamma-ray production cross sections for carbon and nitrogen from threshold to 20.7 MeV, *Nucl. Sci. Eng.*, *58*, 298–313, 1975.

Share, G. H., and R. J. Murphy, Atmospheric gamma rays from solar energetic particles and cosmic rays penetrating the magnetosphere, *J. Geophys. Res.*, *106*, 77–92, 2001.

Share, G. H., R. L. Kinzer, J. D. Kurfess, D. C. Messina, W. R. Purcell, E. L. Chupp, D. J. Forrest, and C. Reppin, SMM detection of diffuse Galactic 511 keV annihilation radiation, *Astrophys. J.*, *326*, 717–732, 1988.

Share, G. H., R. L. Kinzer, M. S. Strickman, J. R. Letaw, E. L. Chupp, D. J. Forrest, and E. Rieger, Instrumental and atmospheric background lines observed by the SMM Gamma Ray Spectrometer, in *High Energy Radiation Background in Space: AIP Proceedings*, vol. 186, edited by A. C. Rester Jr. and J. I. Trombka, pp. 266–277, AIP, New York, 1989.

Shea, M. A., and D. F. Smart, Fifty years of cosmic radiation data, *Space Sci. Rev.*, *93*, 229–262, 2000.

Wigmans, R., PeV cosmic rays: A window on the leptonic era?, *Astroparticle Phys.*, *19*, 379–392, 2003.

Willett, J. B., and W. A. Mahoney, High spectral resolution measurement of gamma ray lines from the Earth's atmosphere, *J. Geophys. Res.*, *97*, 131–139, 1992.

M. J. Harris, Universities Space Research Association, 1101 17th Street N.W., Suite 1004, Washington, D. C. 20036, USA. (harris@osse.nrl.navy.mil)

M. D. Leising, Department of Physics and Astronomy, Clemson University, Box 1911, Clemson, SC 29634-1911, USA. (lmark@clemson.edu)

G. H. Share, Code 7652, Naval Research Laboratory, Washington, D. C. 20375-5320, USA. (share@ssd5.nrl.navy.mil)